

Seasonal predictability of high sea level frequency using ENSO patterns along the U.S. West Coast

ABDOU KHOUAKHI¹, GABRIELE VILLARINI², WEI ZHANG², LOUISE J. SLATER³

¹ School of Architecture, Civil and Building engineering, Loughborough University, Loughborough, UK

² IIHR-Hydroscience & Engineering, The University of Iowa, Iowa City, Iowa, USA

³ School of Geography and the Environment, University of Oxford, UK

Correspondence: a.khouakhi@lboro.ac.uk

ORCID: 0000-0002-1224-3208

Abstract

High sea levels can be conducive to coastal flooding, coastal erosion and inland salt-water intrusion, and thus pose a significant threat to coastal communities, ecosystems and coastal assets. Increases in high water levels have been attributed largely to rising mean sea levels associated with intra-seasonal to interannual climate modes of variability such as the El Niño-Southern Oscillation (ENSO). Here, we examine the predictability of the seasonal frequency of high sea levels using the Niño3.4 index. Different high sea level quantities are considered at 23 tide gauges along the U.S. West Coast, including storm surge and nuisance (minor) floods. At each site, we develop a statistical probabilistic forecasting model for seasonal high sea level frequency during the cold period of October-March. As predictors, we compare the use of (1) seasonal Niño3.4 index observations over the warm antecedent period of July-September and (2) seasonal Niño3.4 index forecasts from the North American Multi-Model Ensemble (NMME) over the cold concurrent period of October-March. Results indicate that the Niño3.4 observations are a good predictor of seasonal high sea level frequency, especially for predicting the storm surge frequency. Correlation coefficients between the observed and modelled seasonal storm surge frequency range from 0.6 to 0.95 at most of the 23 tide gauges. In the predictive model, when using NMME Niño3.4 index, correlation coefficients range between approximately 0.4 and 0.7 at the southern gauges for Niño3.4 index forecasts initialized from October to June (the skill decreases with lead time). Our results provide insights into the seasonal predictability of high sea levels using ENSO patterns which is important for planning and coastal management.

Keywords: high sea level; Niño3.4; NMME; nuisance floods, storm surges

1. Introduction

Coastal communities, ecosystems and infrastructure are under threat of extreme sea level events and flood risk in many parts of the world. Extreme sea levels are generated mainly by the interaction of mean sea level, high tides and storm surges (Pugh and Woodworth, 2015). The term *mean sea level* (MSL) refers to the average level of the sea over a given period, relative to the land; *storm surges* are high water levels caused by abrupt changes in atmospheric pressure and wind (e.g., tropical and extratropical storms). Globally, it is estimated that about 200 million people are currently living in areas vulnerable to extreme sea levels from storm surge flooding. That number is expected to increase to 800 million by 2080 due to the increase in coastal population (Nicholls, 2010). Such a rise in sea level is likely to exacerbate the effects of major storms on coastal communities and infrastructure.

Extreme sea levels have increased worldwide and their interannual fluctuations are driven by changes in regional climate patterns processes such as the El Niño-Southern Oscillation (ENSO, Menéndez and Woodworth, 2010). Along the U.S East and West Coasts, El Niño conditions are found to increase mean sea levels and frequency of high storm surges. These conditions also cause minor (nuisance) flooding when they coincide with high tides (Sweet *et al.*, 2014). Recent analysis of tide gauge data indicated that nuisance flood frequencies were amplified at 49 locations along the U.S. West and East coasts during the El Niño phase of ENSO (Sweet *et al.*, 2018). Overall, it is now well documented that regional sea level variability is associated with climate modes such as ENSO (e.g., Bromirski *et al.*, 2003, 2011; Hamlington *et al.*, 2015; Roberts *et al.*, 2016; Sweet and Zervas, 2011; Thompson *et al.*, 2013; Wahl and Chambers, 2016; Zhang and Church, 2012).

Seasonal high sea level (HSL) forecasting is an important tool for coastal planning and decision-making. The forecasts can be used for preparedness and awareness purposes, as well as to inform annual budgeting, and to help establish proactive responses strategies. Hence, it is important to be able to predict the occurrence of HSLs, including nuisance (minor) floods that cause damage to low-lying infrastructure such as commercial properties, houses, harbors and beaches. Existing research has principally focused on projecting long term changes in coastal flooding (Cayan *et al.*, 2008; Church *et al.*, 2013; Little *et al.*, 2015; Slangen *et al.*, 2014), but less is known about the predictability of HSLs at shorter (i.e., seasonal) time scales.

The predictability of sea levels has been examined using either dynamical or statistical approaches. Dynamical models have been used to investigate the predictability of sea level on seasonal timescales (e.g., McIntosh *et al.*, 2015; Miles *et al.*, 2014; Roberts *et al.*, 2016). For example, dynamical coupled ocean-atmosphere models have been used to predict seasonal sea level anomalies globally with a lead time of up to seven months (Miles *et al.*, 2014). Skillful forecasts of sea level anomalies have been obtained for coastal locations in the tropical Indian and Pacific Oceans up to eight months ahead, based on the dynamical Predictive Ocean Atmosphere Model (McIntosh *et al.*, 2015). Observations have even been combined with eddy-permitting global

circulation model experiments to evaluate the drivers and predictability of dynamical sea levels on seasonal-to-interannual timescales, using 15 leading modes of climate variability in the Atlantic, Indian, Pacific, and Southern Oceans (Roberts *et al.*, 2016).

Statistical approaches have also proven useful in predicting sea levels (Chowdhury *et al.*, 2007; Chowdhury and Chu, 2015). These methods depend on historical time series of training data to predict the sea level variability at a given tide gauge. Such approaches have shown that ENSO and sea surface temperature (SST) are primary factors in modulating sea level variability in the tropical Pacific Ocean on seasonal time scales (Chowdhury *et al.*, 2007). The authors used canonical correlation analysis to forecast sea levels over seasonal time scales (3- to 5- month lead times) in the U.S. affiliated Pacific Islands. The model was later improved over longer forecast horizons by adding zonal wind as a predictor (Chowdhury and Chu, 2015).

In this study, we focus on the usefulness of ENSO patterns for predicting HSL frequency at tide gauges along the U.S. West Coast. The aims of this paper are thus to: (1) develop probabilistic models relating the occurrence of October-March HSL events at tide gauges along the U.S. West Coast to the concurrent ENSO conditions; (2) quantify the skill of the observed October-March and the lagged July -September ENSO in forecasting seasonal HSL occurrences at locations where ENSO was an important predictor.

2. Data and methodology

2.1 Data

We use hourly tide gauge data obtained from the Center for Operational Oceanographic Products and Services of the National Oceanic and Atmospheric Administration (CO-OPS NOAA). We selected 23 gauges along the U.S. West Coast that have over 25 complete years of data between 1984 and 2018. A year is defined as starting in July, and a complete year is one with over 90% of hourly measurements each year (**figure 1**).

We consider three sea level quantities for each tide gauge to evaluate where the ENSO signal is the strongest:

- the raw sea level time series that include both the tidal and seasonal mean sea level cycles (*raw sea level*);
- the time series representing storm surges, obtained after removal of the tidal oscillation component from the raw sea level observations (i.e. non-tidal residuals);
- the time series obtained after removal of both the tidal oscillations and the mean sea level seasonality (i.e. raw sea level minus MSL minus tides, *smt*).

Mean sea level variability is accounted for by subtracting the monthly sea level moving median at each tide gauge record. The removal of tidal oscillations from the observed sea level time series is accomplished by applying a tidal harmonic analysis at each tide gauge record using the 37 NOAA tidal constituents. We use the *TideHarmonics* R package (Stephenson, 2016) to run the harmonic analysis.

Next, we use the daily highest water levels exceeding a given threshold to define HSL frequency. Two threshold levels have been used at each tide gauge (**figure 2**):

- The nuisance flood threshold level (used only for the *raw* sea level time series), i.e. the minor flood threshold established by the NOAA National Weather Service at each gauge. Nuisance flood events are considered a growing problem at many locations along the U.S. coastline and are increasing in frequency (e.g. Sweet and Park, 2014; Vitousek *et al.*, 2017). Since there are only five gauges in the study area that have a defined official nuisance flood threshold (**figure 1**), we derived the rest of the nuisance threshold proxies by using a linear relationship between the official NOAA thresholds and the great diurnal tide range (GT) tidal datum (which refers to the difference in height between the mean higher high water (MHHW) tidal datum and the mean lower low water (MLLW) tidal datum) (following Sweet *et al.* (2018), i.e. *estimated nuisance level* = $1.04 * GT + 0.5$ m; see Sweet *et al.* (2018) for detail on the threshold estimation approach). **Table S1** in the supplemental materials indicates the official and derived thresholds for each of the considered tide gauges in this study.
- The 99.5th percentile of the distribution of the three different sea level quantities (i.e. *raw*, *non-tidal*, and *smt* time series).

We compute the total annual number of days exceeding these thresholds over the cold season (from October to March) to produce four time series of seasonal sea level exceedance days denoted hereafter by *nuisance*, *sl₉₉₅*, *res₉₉₅* and *smt₉₉₅*. *Nuisance* stands for the raw sea level days exceeding the nuisance threshold. *sl₉₉₅*, *res₉₉₅* and *smt₉₉₅* denote raw sea level days, non-tidal residual (storm surges) days and *smt* days exceeding the 99.5th percentile threshold respectively. We choose October - March period because most of highest water levels along the West Coast occur during that cold period (Menéndez and Woodworth, 2010; Sweet *et al.*, 2018).

The SST data are obtained from the Met Office Hadley Center (HadISST; Rayner *et al.*, 2003). From these data, we aggregated the SST values over two separate periods: (a) the cold season (*concurrent* October-March) SST average for every year (year starts in July), at each pixel globally; (b) the warm season (*antecedent* July- September) average SST for every year, at each pixel globally. We use the warm lagged SST to test whether there is greater predictability from using observed *preceding* SSTs in comparison with the ENSO forecasts over the *concurrent* period (see the following section). Recent studies have shown that the predictability of hydroclimatology

over North America can be increased when considering antecedent Pacific SSTs (from preceding seasons of the target season) (e.g. DelSole and Banerjee, 2017; Mamalakis *et al.*, 2018).

The observed Niño3.4 SST index are obtained from the Global Climate Observing System Working Group on Surface Pressure (Rayner *et al.*, 2003)

2.2 Modeling the relationship between HSLs and SSTs/ Niño3.4 index

To examine the predictability of HSLs from Niño3.4 over the cold season (October-March), we first model the four sea level quantities (*nuisance*, *sl995*, *res995* and *smt995*) at every tide gauge using concurrent and preceding SSTs as the predictor at each SST pixel globally. At tide gauges where a significant relationship is found with SST anomalies in the central Pacific (Niño3.4 region), we then model the sea level quantities using the Niño3.4 index.

In all cases, we model the number of days exceeding the thresholds described in section 2.1 using negative binomial regression (NBR; Hilbe, 2011) in a probabilistic framework based on Generalized Additive Models for Location, Scale and Shape (GAMLSS) (Rigby and Stasinopoulos, 2005; Stasinopoulos and Rigby, 2015). We chose a NBR model instead of the more conventional Poisson regression because of the discrete nature of the sea level data and the large variability in the data. We found that the sea level variability is too large to be described by a Poisson distribution, where the mean and the variance are the same, and the Poisson distribution can be viewed as a special case of the negative binomial distribution. We write N_i as the number of hours exceeding a threshold in the i^{th} year. N_i has a conditional negative binomial distribution (Rigby and Stasinopoulos, 2005):

$$P(N_i|\mu_i, \sigma_i) = \frac{\Gamma(N_i + (\mu_i/\sigma_i))\sigma_i^{N_i}}{\Gamma(\mu_i/\sigma_i)\Gamma(N_i+1)(1+\sigma_i)^{N_i+\mu_i/\sigma_i}} \quad (1)$$

where $N_i = 0, 1, 2, \dots, \infty$, $\mu_i > 0$ and $\sigma_i > 0$. In this parameterization, the mean is equal to the parameter μ_i , and the standard deviation is equal to $\sqrt{(1 + \sigma_i)\mu_i}$. The parameter σ_i is a dispersion parameter that allows us to describe the over-dispersion in the data, with Poisson regression being a special case as $\sigma_i \rightarrow 0$. We consider linear dependencies between the parameters μ_i and σ_i and the covariate $x_{sst/Niño}$ (the October-March and July-September SST anomalies, i.e. Niño3.4 index):

$$\begin{cases} \mu_i = \exp(\beta_0 + \beta_1 x_{sst/Niño,i}) \\ \sigma_i = \exp(\gamma_0 + \gamma_1 x_{sst/Niño,i}) \end{cases} \quad (2)$$

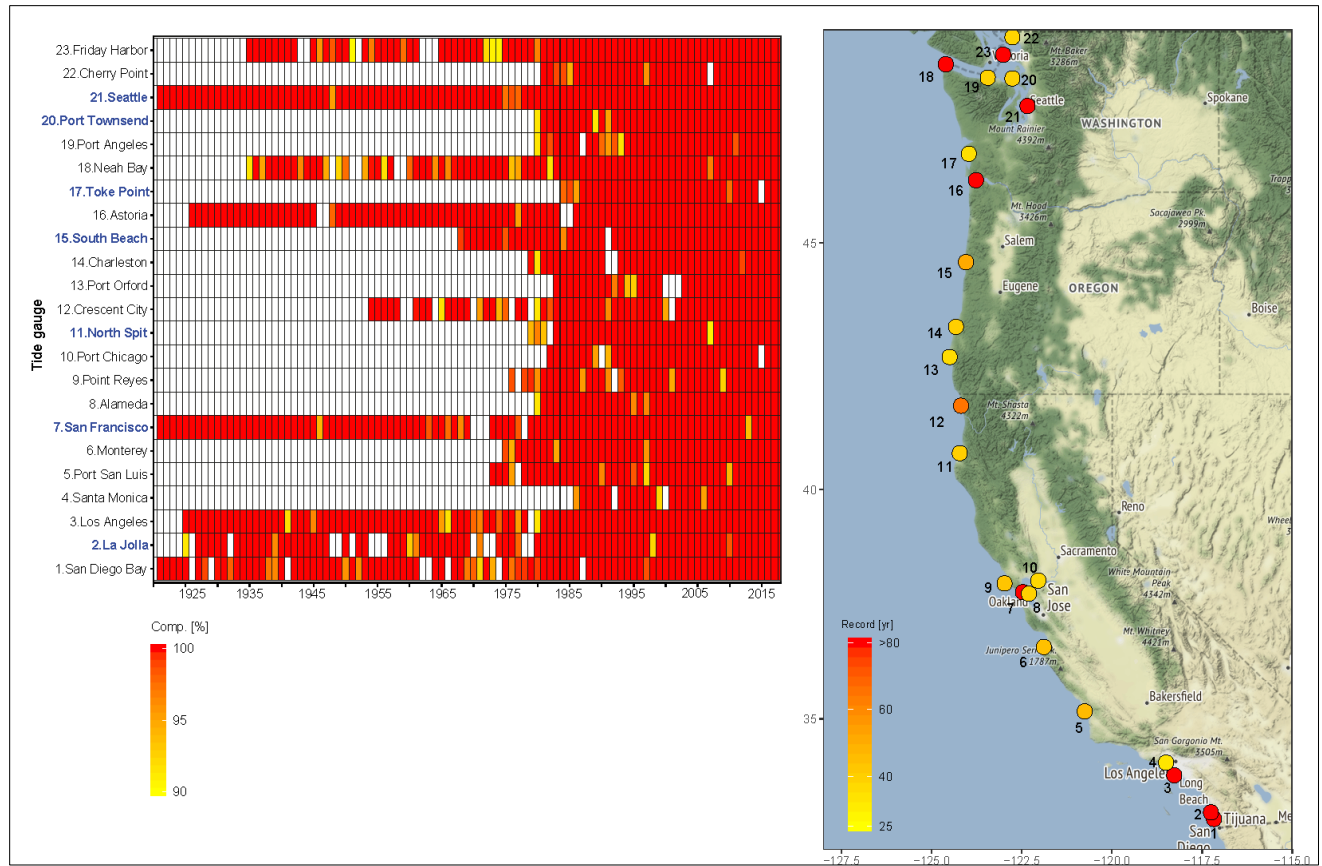
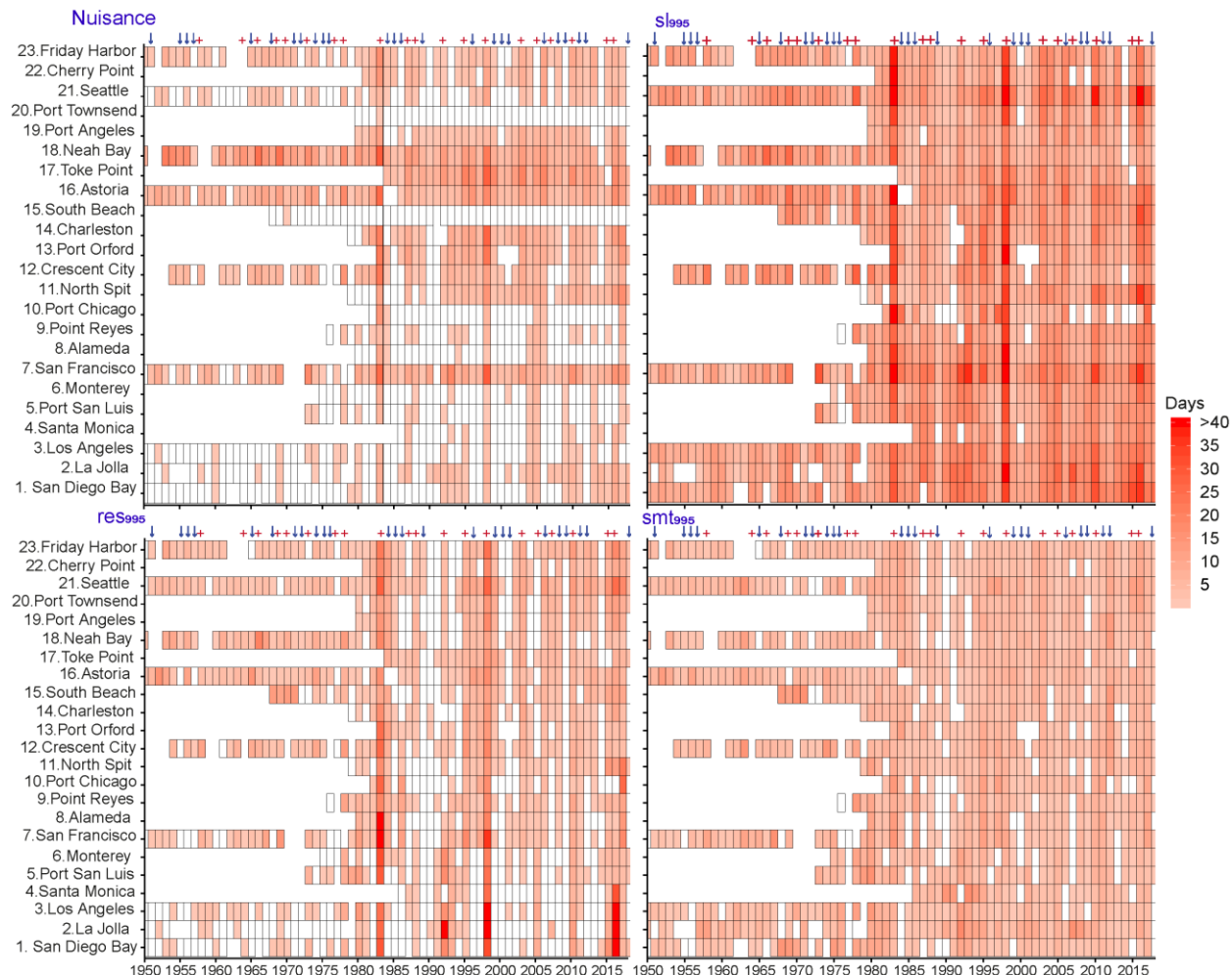


Fig. 1. The 23 selected tide gauges with at least 25 complete years between 1984 and 2018. The left panel indicates the period of record for each tide gauge with the completeness of the hourly data for every year (90% completeness is the minimum considered here). Site names in bold blue font denote tide gauges with official nuisance flood thresholds. The right panel indicates the geographic location of the 23 tide gauge stations. The numbers on the map match those in the left panel.

172



173

174

175

176

177

178

179

180

181

182

183

184

185

186

Fig. 2. Number of HSL days exceeding different thresholds.

Each of the four panels indicates a different sea level quantity. The y-axis indicates the different tide gauge stations (rows) and their numbers; x-axis the years. The shade of red indicates the number of days above each threshold, ranging from no days (white) to more than 40 days per year (red). Years with above-average sea levels appear as red vertical columns on the color maps. Red crosses (blue arrows) on top of each panel indicate years with moderate to strong El Niño (La Niña) where absolute value of Niño 3.4 index exceeding 0.5. The record length for tide gauges 1,2,3,7,16,18,21,23 starts before 1950 but have been truncated here at 1950 for visualization purposes.

2.3 Niño3.4 index forecasts

October-March Niño3.4 index forecasts are computed using SST outputs from eight coupled global climate models (GCMs) from the North American Multi-Model Ensemble (NMME; Kirtman *et al.*, 2014), as described in (Kumar *et al.*, 2017; Zhang *et al.*, 2017). Hindcasts and forecasts of SST data are obtained from eight models – CanCM3, CanCM4, CCSM3, CCSM4, CFSv2, GFDL CM2.1, GFDL FLOR B01 and NASA-GEOS5 (acronyms defined in **Table 1**). These GCMs provide forecasts of different variables at monthly resolutions, from the early 1980s to the present, with lead times ranging from 0.5 to 11.5 months. We compute the mean SST forecast over the Niño3.4 region (5°S–5°N and 170°–120°W) using all 94 NMME members from the eight GCMs.

We aggregate the Niño3.4 index forecasts over the 6-month period, so for example, a forecast of the October-March Niño3.4 Index initialized in October will be comprised of the average monthly forecast over the six months (i.e. forecasts for October with 0.5-month lead, November with 1.5-month lead, December with 2.5-month lead, January with 3.5-month lead, February with 4.5-month lead, and March with 5.5-month lead).

Table 1: Summary of the characteristics of the NMME models used in the study.

Model and Modeling Center	Available Period	Ensemble Size	Lead Times (months)
CanCM3 3rd Generation Canadian Coupled Global Climate Model, Environment Canada’s Meteorological Service of Canada - Canadian Meteorological Centre	1981 - Present	10	0.5 – 11.5
CanCM4 4th Generation Canadian Coupled Global Climate Model, Environment Canada’s Meteorological Service of Canada - Canadian Meteorological Centre	1981 - Present	10	0.5 – 11.5
CCSM3 Community Climate System Model, version 3, National Center for Atmospheric Research (NCAR), Center for Ocean–Land–Atmosphere Studies (COLA), and Rosenstiel School for Marine and Atmospheric Science, University of Miami (RSMAS)	1982 - Present	6	0.5 – 11.5
CCSM4 Community Climate System Model, version 4 – subset of CESM1; National Center for Atmospheric Research (NCAR), Center for Ocean–Land–Atmosphere Studies (COLA), and Rosenstiel School for Marine and Atmospheric Science, University of Miami (RSMAS)	1982 - Present	10	0.5 – 11.5
CFSv2 Operational Climate Forecast System version 2, National Centers for Environmental Prediction (NCEP)	1982 - Present	24	0.5 – 9.5

Model and Modeling Center	Available Period	Ensemble Size	Lead Times (months)
GFDL CM2.1 Climate Model, version 2.1, NOAA Geophysical Fluid Dynamics Laboratory (GFDL)	1982 - Present	10	0.5 – 11.5
GFDL FLOR B01 Climate Model version 2.5, NOAA Geophysical Fluid Dynamics Laboratory (GFDL)	1980 - Present	12	0.5 – 11.5
NASA-GEOS5 Goddard Earth Observing System Model, version 5, National Aeronautics and Space Administration (NASA) Global Modelling and Assimilation Office (GMAO)	1981 - Present	12	0.5 – 9.5

3. Results

3.1. Model results

High sea level frequencies for each sea level quantity (*nuisance*, *sl₉₉₅*, *res₉₉₅* and *smt₉₉₅*) were modelled at each tide gauge along the U.S. West Coast using a negative binomial regression (NBR) model and SSTs as the predictor (**equation 2**). The model was fit globally at every SST pixel averaged over the October-March (cold season) and July-Sept (preceding warm season). **Figure 3** illustrates the computed relationship between HSL days exceeding each threshold and the predictors (cold season in the top row; warm season in the bottom row) at the Charleston tide gauge, Oregon (supplemental **figure set 1a,1b** indicates the model fit for each of the 23 tide gauges, for both predictors). Note that for some tide gauge stations where there were not enough exceedances *nuisance* distribution, we did not fit the NBR model (**figure 2**).

We find a positive and statistically significant relationship between the number of HSL days exceeding each threshold and the observed SST in the Niño3.4 region for most of the other 22 tide gauge stations (**figure set 1a,1b**). This relationship is illustrated using the μ parameter at the Charleston tide gauge (**figure 3**), where we find a positive relationship between both the preceding July-September and the concurrent October-March SSTs and October-March sea level exceedances for *nuisance*, *sl₉₉₅* and *res₉₉₅*. However, the relationship is less strong when modeling the sea level distribution component with MSL removed (*smt₉₉₅*) (**figure 3**, fourth column).

The positive relationship between high sea level exceedances and SSTs suggests that warmer sea waters in the central and eastern tropical Pacific Ocean correspond to higher sea level frequency. Additionally, these results imply that seasonal sea level frequency along the U.S. West Coast is indeed tied to ENSO patterns which can be an important predictor in modeling the seasonal frequency of high-water levels including nuisance floods and storm surges. Given the weak relationship between SSTs and HSLs after removing the MSL, it appears that ENSO is not an

important predictor when modeling HSLs unrelated to MSL. In other words, ENSO relates to the frequency of HSLs primarily via its influence on mean sea levels.

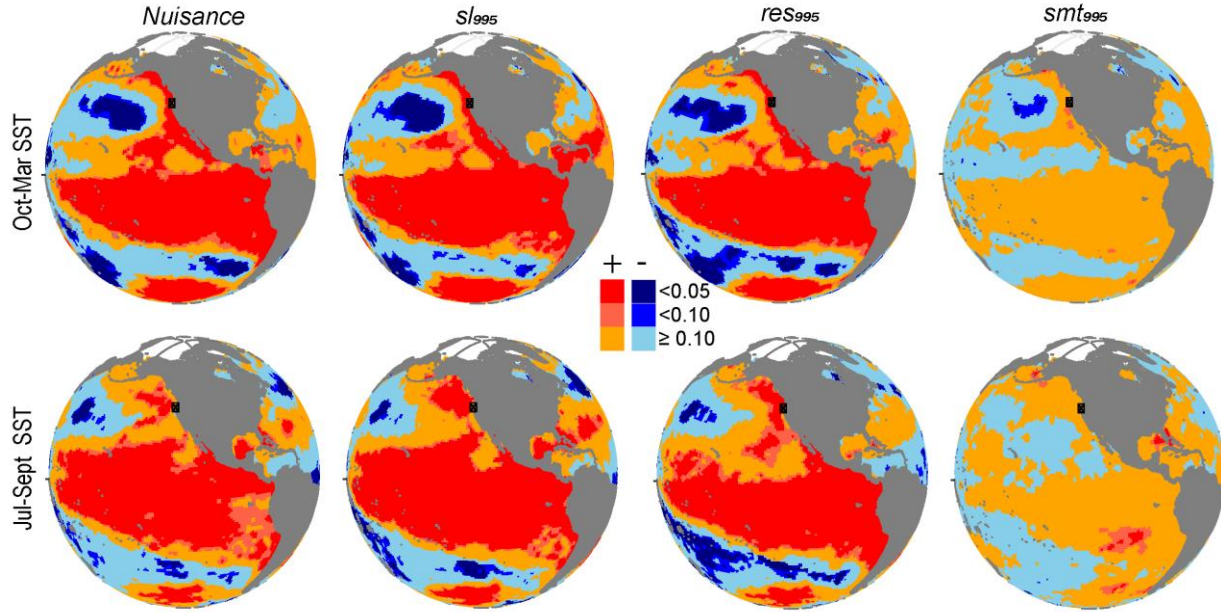


Fig. 3: The relationship between the number of HSL days exceeding each threshold and the average SST for periods of October-March (top row) and lagged July-September (bottom row) at the Charleston tide gauge, Oregon, USA. The Charleston tide gauge is indicated as a black square. The first and second columns indicate frequency of exceedance of the nuisance flood level (*nuisance*) and of the 99.5th percentile of the sea level distribution (*sl995*). The 3rd and 4th columns refer to the same relationships but after the removal of the tidal component (*res995*), and after removing both the tidal and MSL components from the sea level data (*smt995*). Results are shown for the μ parameter (the dependence of the σ parameter on SST is much weaker). For each SST pixel, the only predictor for the negative binomial regression model is the SST. The red (blue) colors point to a positive (negative) relationship between the μ parameter of the negative binomial distribution and SST. Darker shades of red and blue indicate results that are significant at the 5% and 10% level (see color bar).

Given the existence of a significant positive relationship between SST in the Niño3.4 region and HSLs (i.e. *nuisance*, *sl995* and *res995*) at most of the tide gauges, we evaluate how well this relationship describes the year-to-year variations in these quantities. Specifically, we fit a negative binomial regression model using the observed Niño3.4 SST index (averaged over the concurrent October-March and the antecedent July-September periods) as explanatory variable for the sea level exceedance data (**figure 4, figure set 2a, 2b**).

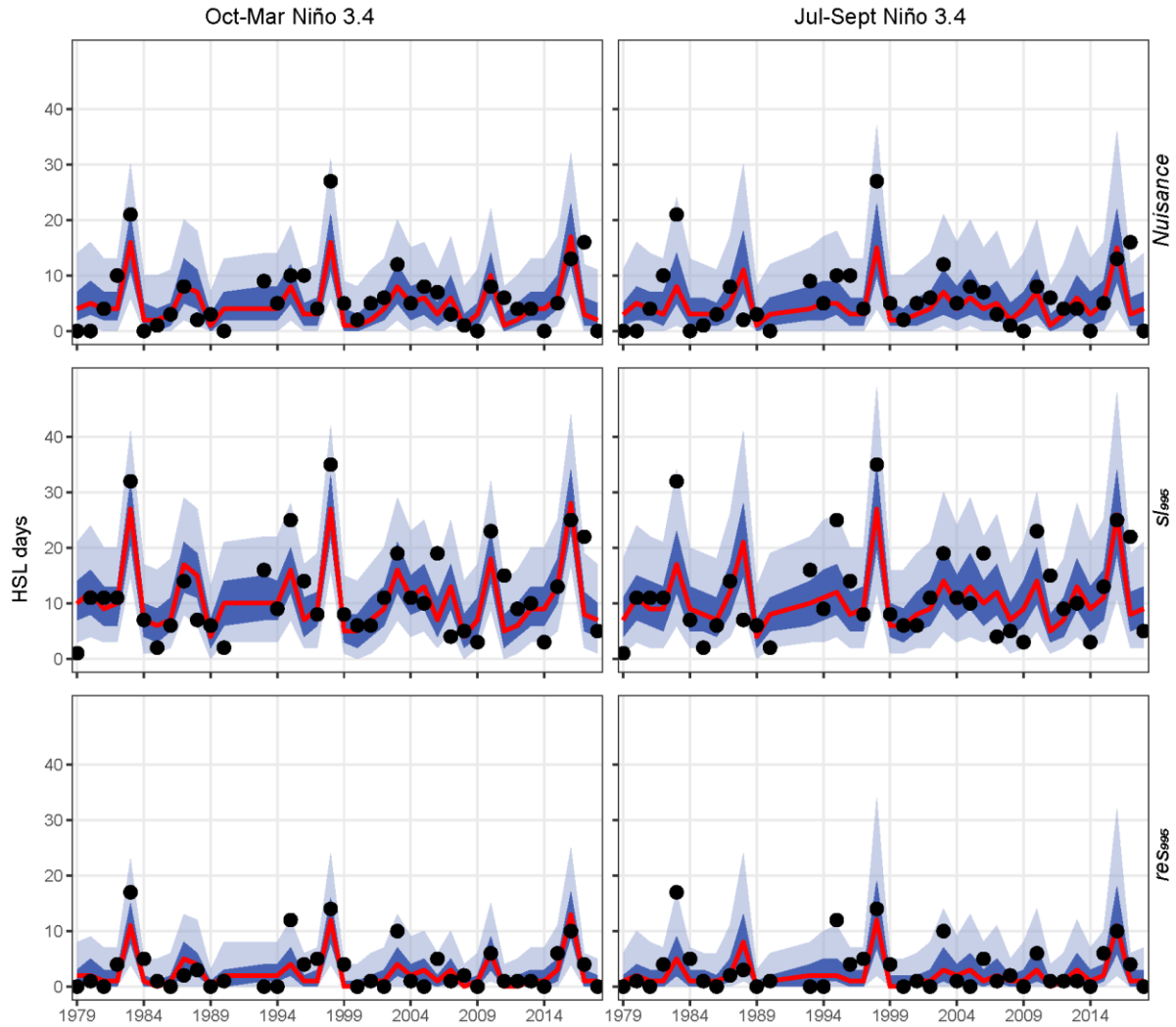


Fig. 4: Example of statistical modeling of sea level exceedance days above different thresholds (rows) at the Charleston tide gauge during October-March, using Niño3.4 as predictor averaged over the periods October-March (left column) and July-September (right column). Black circles indicate observed values of seasonal sea level frequency, i.e., number of HSL exceedance days above the nuisance flood level (*nuisance*; **first row**) and above the 99.5th percentile of the sea level distribution (*sl995*; **second row**). The bottom row shows the same data but after removing the tidal component (*res995*). The colored ribbons in the background indicate the modeled probability distribution for every year. The red line represents the median (50th percentile), the blue ribbon represents the 25th-75th percentiles, and the pale blue ribbon represents the 5th-95th percentiles of the fitted distribution. Results for all other tide gauges are indicated in the supplementary materials figure set 2a, 2b.

Across the 23 gauges, the probabilistic NBR models capture the interannual variations in sea level data well and are consistent with results obtained from the relationship between SST and sea level frequency of *nuisance*, *sl995* and *res995* (**figure 3**). We find differences in the model fit depending on whether we focus on the exceedances above the nuisance level or above the 99.5th percentile of the sea level distributions (**figure 4**). Moreover, results indicate that both the concurrent and the antecedent Niño3.4 can be used to forecast seasonal sea level exceedances at the Charleston tide gauge. Correlations between the median modeled probability distribution and observed seasonal HSLs at the Charleston tide gauge using concurrent (preceding) Niño3.4 are about 0.72, 0.74, 0.76 (0.59, 0.64, 0.60) for *nuisance*, *sl995* and *res995* respectively with correlations significant at the 5% level.

We summarize the model performance at all 23 tide gauges using the 50th percentile of the modelled probability distribution of seasonal sea levels in a Taylor diagram in **figure 5** (Taylor, 2001). Each panel indicates the correlation coefficients, centered root mean square between observed and modelled seasonal sea level exceedances and their normalized standard deviations for each sea level quantity (i.e *nuisance*, *sl995* and *res995*). At most of the 22 tide gauges the correlation coefficients between modelled and observed sea level exceedances range between 0.4 and 0.95. The best scores in terms of correlation coefficients and RMSE are obtained when modelling storm surge (*res995*) exceedances. The sites with the best model fits are the tide gauges located along the southern U.S. West Coast (i.e San Diego bay, La Jolla, Los Angeles, Santa Monica). For nuisance floods the scores are generally lower than for the other sea level quantities. However, we find good model fits at several tide gauges (e.g. 4, 14, 17, 2), with the correlation coefficients varying between 0.5 and 0.72. It can also be seen that the standard deviations of the fitted distributions are generally lower than the standard deviations of the observed values. The model that uses the concurrent observed cold season October-March Niño3.4 as predictor slightly outperforms the one that uses of the preceding warm July-September Niño3.4 in modelling the HSLs in all metrics including the standard deviation ratio, as one might expect.

Overall, these results indicate that both October-March Niño3.4 forecasts and observed (lagged) July-September Niño3.4 can describe seasonal HSLs at many tide gauges along the U.S. West Coast. The advantage of using the observed July-September Niño3.4 is that it can be used directly to forecast sea levels at the tide gauges without having to rely on GCM forecasts to predict Niño3.4 (which might also add to the uncertainties of the model).

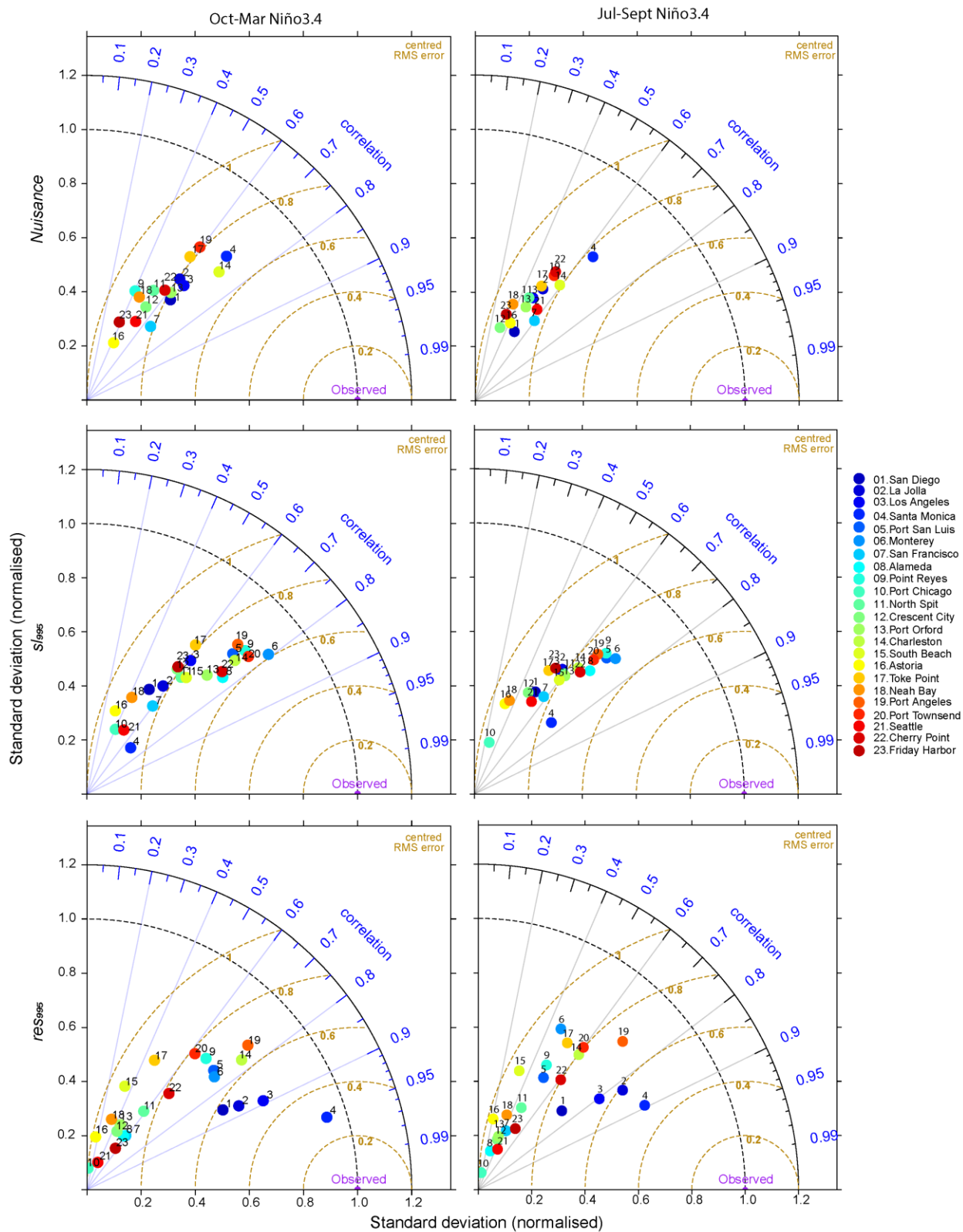


Fig.5. Taylor diagrams summarizing the relationship between the observed values and the median of the modelled sea level exceedances

at each of the 23 tide gauges (circles) for each sea level quantity (rows). The two ENSO predictors (October-March Niño3.4 and July-September Niño3.4) are indicated in the left and right columns respectively, with the sea level quantities on each row. The radial distance represents the ratio of modelled to observed standard deviations (standard deviations are normalized to enable the comparison across tide gauges; the dashed black line shows the normalized standard deviation of the observation; values closer to one indicate a better fit). The azimuthal angle represents the correlation between the modelled and the observed HSL. The orange arcs represent the centered root mean square difference between modelled and observed values. Different gauges are indicated by colored circles and their corresponding numbers (numbering starts from the South).

3.2. Forecast results

The modelling results indicated that the model with the concurrent cold season October-March Niño3.4 performed slightly better than the model using the antecedent warm season July-September Niño3.4. Here we investigate the use of seasonal forecasts of the cold season October-March to assess whether it is possible to predict HSLs several months ahead. To do so, we first compute the NMME forecasts of the October-March Niño3.4 Index (Methods). We find that the skill of the mean raw October-March Niño3.4 Index forecast ranges from a correlation coefficient of 0.91 when the forecast is initialized in October (just before the onset of Niño3.4) and decreases (as the lead time increases) to 0.69 when the forecast is initialized in April (6.5 months before the onset of Niño3.4) (Table 2).

Table 2: Skill of NMME-based Niño 3.4 forecasts with various lead times. The skill is computed between the mean of the Niño3.4 seasonal forecasts (computed as described in the Methods) and the observed seasonal values.

Initialization month	R	R ²	RMSE
October	0.91	0.83	0.42
September	0.88	0.77	0.50
August	0.84	0.70	0.55
July	0.82	0.67	0.58
June	0.78	0.61	0.62
May	0.75	0.56	0.65
April	0.69	0.47	0.72

The mean NMME-Niño 3.4 index forecast (mean of all the available GCM members) is used as the predictor in the models described in **section 2.1**. The model is trained using the observed Niño3.4 index over 70% of each historical gauge record (note: the length of the record varies

depending on the gauge). We store the parameters from the trained model and use them to compute the sea level exceedance forecast, using the NMME-Niño3.4 index forecast value as the predictor on the remaining 30% of each gauge record (we also trained the model using 80% of each gauge record and tested on the remaining 20%, results are provided in the **figure S3** in the supplemental material with correlation scores showed some differences but similar patterns across sites). The overall forecasting performance is evaluated by comparing the median of the probabilistic forecast distribution (for each lead time) and the observations, for every sea level quantity (i.e. *nuisance*, *sl995*, *res995*) and for all tide gauges.

Figure 6 summarizes the forecast skill using the correlation coefficient and RMSE between the observations and the median of the forecast distribution of sea level frequency at each tide gauge and for each sea level quantity. Overall, the highest correlation scores are recorded at the southern tide gauges (e.g. La Jolla, San Diego, Los Angeles, Santa Monica, San Francisco). We find that the forecasts are more skillful for the highest storm surge and for the highest raw sea level frequencies compared to the *nuisance* flood frequency.

Correlation scores for storm surge frequency are relatively high, and range between ~ 0.5 and 0.8 at the southern gauges (California gauges) across all initialization times. Overall, the forecast skill does not exhibit a perfect monotonic decrease as the initialization time increases (**figure 6**). However, there are some gauges, such as the San Francisco gauge, where the forecast skill does decrease broadly with increasing initialization time (from 0.7 in October, 1 month ahead, to 0.53 in April, 6.5 months ahead of the period of interest). If we consider the raw sea level frequencies (*sl995*), the forecast skill is also higher in the southern gauges, but the correlation scores are slightly lower than for *res995* (from ~ 0.35 to 0.82 ; **figure 6**, 2nd row). Nuisance forecasts are typically weaker than the high sea level (*sl995*) and storm surge forecasts: R ranges between 0.3 and 0.4 broadly, except at the San Francisco gauge where $R = 0.7$ for the Niño3.4 index forecast initialized in August (2.5 months ahead). Overall these results indicate that NMME Nino 3.4 forecasts can be used to estimate seasonal sea level frequency with most accuracy in California and for the seasonal storm surge frequency (compared to the other sea level quantities).

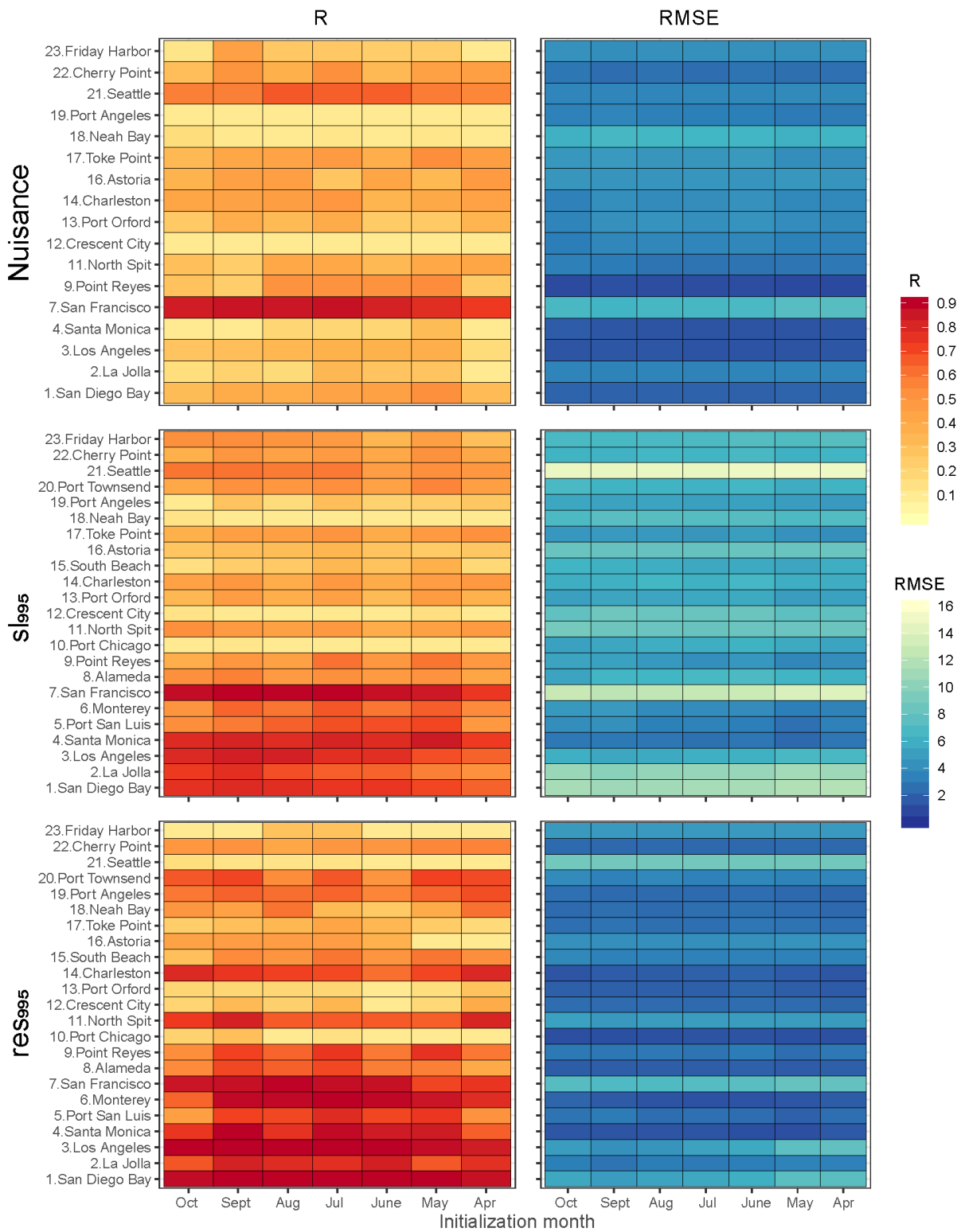


Fig. 6: Performance of the seasonal forecast of flood level exceedances at the 23 U.S. West Coast tide gauges during the October-March period, using the October-March Niño3.4 index forecasts. The performance is evaluated by comparing the median of the forecast

distribution for each lead time (x-axes indicate) and the observations, for every sea level quantity. Panels of the left column (red shades) indicate the correlation coefficient scores; right column indicate the RMSE (blue shades); y-axes indicate the 23 tide gauges. Each row indicates a different sea level quantity *nuisance*, *sl₉₉₅*, *res₉₉₅* respectively.

4. Summary and Conclusions

The primary goal of this study has been to examine the use of ENSO patterns and sea surface temperature fluctuations in the tropical Pacific Ocean in predicting high sea level frequency at the seasonal time scale in tide gauges along the U.S West Coast. As outlined in the introduction, several studies have shown substantial year-to-year variability in sea levels along the US West Coast induced by the influence of ENSO on weather and ocean circulation patterns. Our proposed NBR model shows potential in capturing these variabilities in HSL frequency at seasonal scales.

We find statistically significant relationships between seasonal HSL frequency and variations of tropical Pacific SSTs (and subsequently the Niño 3.4 index) at most of the 23 tide gauges. Using the Niño3.4 index, we find that the predictability of the seasonal HSL frequency varies at each tide gauge and across different sea level components. The ENSO signal is better captured when we focus on seasonal high storm surge frequency compared to raw sea level (*sl₉₉₅*) or nuisance exceedances, because the tidal component highly influence both *sl₉₉₅* and *nuisance* high waters (Sweet *et al.*, 2018). Higher model skills are found in the southern tide gauges of California. One possible explanation for this higher skill is the stronger signal of ENSO during El Niño winters, when the storm track and Pacific jet displace southward over the eastern Pacific (Seager *et al.*, 2010), affecting the southern/southwestern United States and Mexico. The resulting storm surges can cause damage and induce nuisance floods, especially if they occur during high tides (Sweet *et al.*, 2018, 2014).

As one would expect, when removing MSL variability, the predictability of HSLs is significantly reduced in most of the gauges since much of the ENSO-related sea level variability that contributes to high water is removed by the subtraction of the monthly median sea level.

The model fit is slightly better across tide gauges using the concurrent October-March Niño3.4 index rather than the index during the antecedent warm July-September period. However, in term of predictions, using the observed antecedent Niño3.4 index as a predictor of seasonal HSL frequency instead of using GCM cold season forecasts will have the benefit of reducing any uncertainty associated with the forecasts.

In conclusion, the main results can be summarized as follows:

- There is an association between ENSO and the seasonal frequency of HSLs. This relationship is well captured through negative binomial regression models developed for different HSL quantities.

- Our proposed NBR-Niño3.4 based model provides valuable skill for predicting seasonal HSL frequency along the U.S West Coast. The seasonal high storm surge frequency is the component with the greatest predictability. We find higher forecasting skill in the southernmost tide gauges.
- The Niño3.4 index can be used to predict HSLs ahead of the October-March cold season both: (1) by using NMME Niño3.4 index cold season forecasts and (2) by using the antecedent warm season Niño3.4 index observation.
- The NMME forecasts of the October-March Niño3.4 index can be used to predict exceedance of the seasonal HSLs with lead times of up to 6 months at some tide gauges. However, the skill decreases as the Niño3.4 forecast lead time increases, as would be expected. Further improvements could be achieved by developing weighted average schemes that leverage the performance of different models at different lead times.

These results have important implications for coastal management and can be used for hazard mitigation response, as well as to inform annual budgeting in flood prone locations, and for emergency mobilizations and proactive response.

Acknowledgments

The authors thank two anonymous reviewers for comments and suggestions that have notably improved the manuscript. The hourly water level data were downloaded from NOAA's Tides and Currents website (<https://tidesandcurrents.noaa.gov>). Gabriele Villarini acknowledges financial support from the National Science Foundation CAREER Grant AGS-1349827 and the USACE Institute for Water Resources.

Supplementary Figure set 1a and 1b, Figure set 2a and 2b, Figure S3 and Tables S1 are available in the Supplementary Materials.

References

- Bromirski PD, Flick RE, Cayan DR. 2003. Storminess variability along the California coast: 1858-2000. *Journal of Climate* **16**(6): 982–993. DOI: 10.1175/1520-0442(2003)016<0982:SVATCC>2.0.CO;2.
- Bromirski PD, Miller AJ, Flick RE, Auad G. 2011. Dynamical suppression of sea level rise along the Pacific coast of North America: Indications for imminent acceleration. *Journal of Geophysical Research: Oceans* **116**(7): 1–13. DOI: 10.1029/2010JC006759.

430 Cayan DR, Bromirski PD, Hayhoe K, Tyree M, Dettinger MD, Flick RE. 2008. Climate change
431 projections of sea level extremes along the California coast. *Climatic Change* **87**: 57–73. DOI:
432 10.1007/s10584-007-9376-7.

433 Chowdhury MR, Chu PS. 2015. Sea level forecasts and early-warning application expanding
434 cooperation in the south pacific. *Bulletin of the American Meteorological Society* **96**(3): 381–
435 386. DOI: 10.1175/BAMS-D-14-00038.1.

436 Chowdhury MR, Chu PS, Schroeder T, Colasacco N. 2007. Seasonal sea-level forecasts by
437 canonical correlation analysis - An operational scheme for the U.S.-affiliated Pacific Islands.
438 *International Journal of Climatology* **27**(10): 1389–1402. DOI: 10.1002/joc.1474.

439 Church J a., Clark PU, Cazenave a., Gregory JM, Jevrejeva S, Levermann a., Merrifield M a.,
440 Milne G a., Nerem R., Nunn PD, Payne a. J, Pfeffer WT, Stammer D, Unnikrishnan a. S. 2013.
441 Sea level change. *Climate Change 2013: The Physical Science Basis. Contribution of Working*
442 *Group I to the Fifth Assessment Report of the Intergovernmental Panel on Climate Change*
443 1137–1216.

444 DelSole T, Banerjee A. 2017. Statistical seasonal prediction based on regularized regression.
445 *Journal of Climate*. DOI: 10.1175/JCLI-D-16-0249.1.

446 Hamlington BD, Leben RR, Kim K-Y, Nerem RS, Atkinson LP, Thompson PR. 2015. The effect
447 of the El Niño-Southern Oscillation on U.S. regional and coastal sea level. *Journal of*
448 *Geophysical Research: Oceans* **120**(6): 3970–3986. DOI: 10.1002/2014JC010602.

449 Hilbe JM. 2011. *Negative binomial regression*. Cambridge University Press.

450 Kirtman BP, Min D, Infanti JM, Kinter III JL, Paolino DA, Zhang Q, Van Den Dool H, Saha S,
451 Mendez MP, Becker E. 2014. The North American multimodel ensemble: phase-1 seasonal-to-
452 interannual prediction; phase-2 toward developing intraseasonal prediction. *Bulletin of the*
453 *American Meteorological Society*. American Meteorological Society **95**(4): 585–601.

454 Kumar A, Hu Z-Z, Jha B, Peng P. 2017. Estimating ENSO predictability based on multi-model
455 hindcasts. *Climate Dynamics*. Springer **48**(1–2): 39–51.

456 Little CM, Horton RM, Kopp RE, Oppenheimer M, Vecchi GA, Villarini G. 2015. Joint
457 projections of US East Coast sea level and storm surge. *Nature Climate Change* (September): 1–
458 8. DOI: 10.1038/nclimate2801.

- 459 Mamalakis A, Yu JY, Randerson JT, Aghakouchak A, Foufoula-Georgiou E. 2018. A new
460 interhemispheric teleconnection increases predictability of winter precipitation in southwestern
461 US. *Nature Communications* **9**(1): 1–10. DOI: 10.1038/s41467-018-04722-7.
- 462 McIntosh PC, Church JA, Miles ER, Ridgway K, Spillman CM. 2015. Seasonal coastal sea level
463 prediction using a dynamical model. *Geophysical Research Letters* **42**(16): 6747–6753. DOI:
464 10.1002/2015GL065091.
- 465 Menéndez M, Woodworth PL. 2010. Changes in extreme high water levels based on a quasi-
466 global tide-gauge data set. *Journal of Geophysical Research* **115**(C10): C10011. DOI:
467 10.1029/2009JC005997.
- 468 Miles ER, Spillman CM, Church JA, McIntosh PC. 2014. Seasonal prediction of global sea level
469 anomalies using an ocean-atmosphere dynamical model. *Climate Dynamics*, pages 1–15. DOI:
470 10.1007/s00382-013-2039-7.
- 471 Nicholls RJ. 2010. Impacts of and Responses to Sea-Level Rise. *Understanding Sea-Level Rise*
472 *and Variability*, 17–51. DOI: 10.1002/9781444323276.ch2.
- 473 Pugh D, Woodworth P. 2015. Sea-level Science: Understanding Tides, Surges, Tsunamis and
474 Mean Sea-level Changes. *Cambridge University Press* **56**(3): 394–394. DOI:
475 10.1080/00107514.2015.1005682.
- 476 Rayner NA, Parker DE, Horton EB, Folland CK, Alexander L V, Rowell DP, Kent EC, Kaplan
477 A. 2003. Global analyses of sea surface temperature, sea ice, and night marine air temperature
478 since the late nineteenth century. *Journal of Geophysical Research: Atmospheres*. Wiley Online
479 Library **108**(D14).
- 480 Rigby RA, Stasinopoulos DM. 2005. Generalized additive models for location, scale and shape.
481 *Journal of the Royal Statistical Society: Series C (Applied Statistics)*. Wiley Online Library
482 **54**(3): 507–554.
- 483 Roberts CD, Calvert D, Dunstone N, Hermanson L, Palmer MD, Smith D. 2016. On the drivers
484 and predictability of seasonal-to-interannual variations in regional sea level. *Journal of Climate*
485 JCLI-D-15-0886.1. DOI: 10.1175/JCLI-D-15-0886.1.
- 486 Seager R, Naik N, Ting M, Cane MA, Harnik N, Kushnir Y. 2010. Adjustment of the
487 atmospheric circulation to tropical pacific sst anomalies: Variability of transient eddy
488 propagation in the pacific-north america sector. *Quarterly Journal of the Royal Meteorological*
489 *Society*. DOI: 10.1002/qj.588.

490 Slangen ABA, Carson M, Katsman CA, van de Wal RSW, Köhl A, Vermeersen LLA, Stammer
 491 D. 2014. Projecting twenty-first century regional sea-level changes. *Climatic Change* **124**(1–2):
 492 317–332. DOI: 10.1007/s10584-014-1080-9.

493 Stasinopoulos DM, Rigby RA. 2015. Generalized Additive Models for Location Scale and
 494 Shape (GAMLSS) in R. *Journal of Statistical Software*. DOI: 10.18637/jss.v023.i07.

495 Stephenson A. 2016. Harmonic Analysis of Tides Using TideHarmonics. .

496 Sweet W V., Zervas C. 2011. Cool-Season Sea Level Anomalies and Storm Surges along the
 497 U.S. East Coast: Climatology and Comparison with the 2009/10 El Niño. *Monthly Weather*
 498 *Review* **139**(7): 2290–2299. DOI: 10.1175/MWR-D-10-05043.1.

499 Sweet W V, Dusek G, Obeysekera J, Marra JJ. 2018. Patterns and Projections of High Tide
 500 Flooding Along the U.S. Coastline Using a Common Impact Threshold. *NOAA Technical Report*
 501 *NOS CO-OPS 086* (February).

502 Sweet W V, Park J. 2014. From the extreme to the mean : Acceleration and tipping points of
 503 coastal inundation from sea level rise Earth ’ s Future. *Earth ’ s Future* **2**: 579–600. DOI:
 504 10.1002/2014EF000272.Received.

505 Sweet W, Park J, Marra J, Zervas C, Gill S. 2014. Sea Level Rise and Nuisance Flood Frequency
 506 Changes around the United States. *National Oceanic and Atmospheric Administration*.

507 Taylor KE. 2001. Summarizing multiple aspects of model performance in a single diagram.
 508 *Journal of Geophysical Research Atmospheres*. DOI: 10.1029/2000JD900719.

509 Thompson PR, Mitchum GT, Vonesh C, Li J. 2013. Variability of Winter Storminess in the
 510 Eastern United States during the Twentieth Century from Tide Gauges. *Journal of Climate*
 511 **26**(23): 9713–9726. DOI: 10.1175/JCLI-D-12-00561.1.

512 Vitousek S, Barnard PL, Fletcher CH, Frazer N, Erikson L, Storlazzi CD. 2017. Doubling of
 513 coastal flooding frequency within decades due to sea-level rise. *Scientific Reports*. DOI:
 514 10.1038/s41598-017-01362-7.

515 Wahl T, Chambers DP. 2016. Climate controls multidecadal variability in U. S. extreme sea
 516 level records. *Journal of Geophysical Research: Oceans* **121**(2): 1274–1290. DOI:
 517 10.1002/2015JC011057.

518 Woodworth PL, Blackman DL. 2004. Evidence for systematic changes in extreme high waters
519 since the mid-1970s. *Journal of Climate* **17**(6): 1190–1197.

520 Zhang W, Villarini G, Slater L, Vecchi GA, Bradley AA. 2017. Improved ENSO Forecasting
521 Using Bayesian Updating and the North American Multimodel Ensemble (NMME). *Journal of*
522 *Climate* **30**(22): 9007–9025. DOI: 10.1175/JCLI-D-17-0073.1.

523 Zhang X, Church JA. 2012. Sea level trends, interannual and decadal variability in the Pacific
524 Ocean. *Geophysical Research Letters* **39**(21). DOI: 10.1029/2012GL053240.

525

526